SPE-198617-MS

# Predicting the Amount of Lost Circulation While Drilling Using Artificial Neural Networks: An Example of Southern Iraq Oil Fields

Ahmed K. Abbas, Iraqi Drilling Company; Hussain M. Hamed, Misan University; Waleed Al-Bazzaz, Kuwait Institute for Scientific Research; Hayder Abbas, Missan Oil Company



This paper was prepared for presentation at the SPE Gas & Oil Technology Showcase and Conference held in Dubai, UAE, 21 - 23 October 2019.



## Abstract

Lost circulation is a serious problem that imposes some extra costs to petroleum and gas exploration operations. Substantial technical and economic benefits can be accomplished if the severity and frequency of mud loss are considered during the well planning procedure. This will lead to preventing the occurrence of losses by using treatments/solutions that are applied before entering lost circulation zones. In the present work, new models were developed to predict the amount of lost circulation using artificial neural networks (ANNs). This model was implemented to obtain a deeper understanding of the relations between the losses rate and the controllable drilling variables (i.e., rate of penetration [ROP], flow rate [FR], circulation pressure [CP], weight on bit [WOB], and rotation per minute [RPM]). The losses rate was found to be sensitive to high ROP, FR, and CP, such that increasing these parameters continuously increase the amount of lost circulation. While a slight rise in the losses rate was observed at high WOB and RPM. The proposed ANNs model was used to predict the losses rate for two wells, and comparison plot (actual amount of lost circulation versus predicted) was introduced as a function of depth. An accurate and early prediction of lost circulation has been of great importance to avoid the risks associated with this problem's occurrence.

## Introduction

Lost circulation problem is one of the most challenging problems that drilling engineers have been struggling with for decades (Chen et al., 2017). The occurrence of such a problem can potentially cause of non-productive time and the most expensive drilling problems (Feng and Gray, 2017). It is detrimental because it can not only lead to safety hazards such as wellbore instability, pipe sticking, and blow out but also leads to formation damage, severe permeability impairment, and a substantial decline in production (Nasiri et al., 2017). Lost circulation is likely to occur in highly porous and permeable formations such as gravel, cavernous or vugular, and naturally fractured formations (Razavi et al., 2016; Ezeakacha and Salehi, 2018). Such formations can allow mud particles to penetrate the near-wellbore regions. The degree of losses depends on the size of the formation pores or fracture throats and the sealing properties of the mud in use. Lost circulation events could be classified based on the losses rate into four distinct groups as seepage loss, when the loss rate is 0.5 -1 m3/hr, partial loss, when the loss rate increases from 1 to 10 m3/hr, severe losses,

when the loss rate increases to 15 m3/hr, and complete losses, when the loss rate is more than 15 m3/hr, or there is no returns to the surface (Alsaba et al., 2017).

Stopping lost circulation while it happens is as important as preventing it from taking place because it can save money which has never been expended (Whitfill et al., 2007). Therefore, it is of great significance to identify the loss mechanism of different strata and to establish a prediction model of the lost circulation risk while drilling. However, numerous efforts have been devoted to study lost circulation materials and plugging technology. Depending on field experience and lacking systematic theoretical guidance, the plugging efficiency is still low (Li et al., 2018). Also, there is little focus on the prediction of lost circulation risk, lacking an intelligent prediction model taking into account geological and engineering factors. Conventional prediction method of lost circulation is mainly to identify the vug and fracture system by the seismic method, or to predict the location and structure where lost circulation may occur based on adjacent well data. However, it is far from enough due to the lack of accuracy and detail.

Several factors affect the severity of lost circulation. Generally, these factors can be classified into three categories: drilling parameters, drilling fluid properties, and mechanical earth model (MEM) parameters. Due to the high complexity and nonlinear behavior of these parameters, finding a reasonable analytical solution to predict the amount of lost circulation is not simple (Toreifi et al., 2014). Because of these difficulties and the restriction to have an idea about the severity and frequency of mud loss, machine learning methodologies seem to be an attractive alternative to model this complicated physical process. A key characteristic of machine learning is its ability to recognize complex patterns with good predictive accuracy through a typical learning process (Alkamil et al., 2018). Thus, machine learning can provide intuitive solutions to complicated problems with no need for the formal description of the underlying physics. This method can develop associations, transformations or mappings between objects or data and has proven to have potential in solving problems that require pattern recognition. Among the machine learning methodologies, artificial neural networks (ANNs) is the most powerful and efficient techniques to identify complex relationships based on previous experience with reasonable cost and time (Abbas et al., 2018a).

In this study, artificial neural networks (ANNs) algorithm is employed to analyze drilling data of previously drilled wells in an oilfield of Southern Iraq and then establish an intelligent model to predict the amount of lost circulation while drilling, taking into account both geological and operational parameters.

## Data Acquisition

Preparing database is a challenging and judgmental step in artificial neural networks modeling. The sufficiency and accuracy of each collected data set play an essential role to propose any acceptable model. The performance of the model is related to solely upon the input training pair. The data used in this study are selected according to the specifications given in the previous literature (Abbas et al., 2019a). Previous studies show that the amount of lost circulation is largely dependent on some critical parameters, which can be classified into three types: drilling parameters, drilling fluid properties, and mechanical earth model (MEM) parameters (i.e., the lithology type, rock mechanical properties, pore pressure ($P_P$), fracture pressure ($F_P$), vertical stress ($\sigma_v$), minimum horizontal stress ($\sigma_h$), and maximum horizontal stress ($\sigma_H$)).

### Drilling Parameters

The drilling-related parameters are the measured depth (MD), hole size (HS), rate of penetration (ROP), rotation per minute (RPM), torque (TQ), weight on bit (WOB), flow rate (FR), circulating pressure (CP), formation type and lithology of the rock (LITHO) and wellbore trajectory (azimuth [AZI] and inclination [INC]). These parameters were collected from 385 wells drilled in southern Iraq in different fields. The drilling mechanical parameters (i.e., MD, ROP, RPM, TQ, WOB, FR, and CP) and wellbore trajectory (i.e., AZI and INC) were captured from a real-time sensor, and most of them were taken based on a meter reading. The total numbers of 1,120 cases (datasets) were considered to be valid data, with a normal distribution.

According to the losses rate, the collected datasets can be classified into four categories: 346 lost circulation cases are a partial loss, 239 lost circulation cases are severe losses, 159 lost circulation cases are complete losses, and other 376 cases are points of no lost circulation.

**Drilling Fluid Properties**

Drilling fluids are circulated down the drill string, through the drill bit and then back up the hole in the interstitial space known as the annulus (Davoodi et al., 2018). They may be composed of a simple water-chemical mixture; more complexly formulated drilling mud, $N_2$ foam, or even other unconventional fluids. Mud properties (i.e., mud weight [MW], marsh funnel viscosity [MFV], plastic viscosity [PV], yield point [YP], 10-second gel strength [Gel 10"], 10-minute gel strength [Gel 10'], fluid loss [FL], and solids content [SC]) have been confirmed as significant factors in determining the severity of lost circulation (Agin et al., 2019).

**Rock Mechanical Parameters**

The elastic parameters (such as Young's modulus ($E$) and Poisson's ratio ($v$)) demonstrate the deformation behavior for isotropic elastic materials (Abbas et al 2019b). The dynamic values of these parameters were calculated using compressional acoustic wave velocity ($v_p$) and shear acoustic wave velocity ($v_s$) associated with the bulk density ($\rho$) logs, as follows:

$$E_{Dynamic} = \rho v_s^2 \left( \frac{3v_P^3 - 4v_s^2}{v_P^2 - v_s^2} \right) \tag{1}$$

$$v_{Dynamic} = \frac{v_P^2 - v_s^2}{2(v_P^2 - v_s^2)} \tag{2}$$

However, these dynamic elastic parameters are usually larger than the static properties. For example, the dynamic Young's modulus is about 3 times greater than the static Young's modulus (Mohammed et al., 2018). Therefore, Wang's correlation is normally used in the literature to convert the dynamic Young's modulus to static Young's modulus (Mansourizadeh et al., 2016):

$$E_{Static} = 0.414 E_{Dynamic} - 1.0593 \tag{3}$$

While, the difference between the static and dynamic Poisson's ratio is about 0.05. Accordingly, the static Poisson's ratio is assumed to be the same as the dynamic Poisson's ratio.

Rock strength parameters such as unconfined compressive strength ($UCS$), cohesive strength ($C_o$), internal friction angle ($\varphi$), and tensile strength ($T_o$) indicates to the ability of the rock formation to withstand the in-situ stress environment around the wellbore. Empirical correlations were adopted to calculate the rock strength parameters using geophysical well logs, such as gamma ray (GR), compressional wave transit times (DTCO), shear wave transit times (DTSM), density (RHOZ), and total porosity (PHIT). Further details about estimating rock strength parameters using wireline measurements are comprehensively discussed in the studies conducted by Chang et al. (2006). In this study, the $UCS$, $\varphi$, and $C_o$ were determined using Eqs. 4, 5, 6, and 7, respectively.

$$UCS = 143.8 \exp(-6.95\phi) \tag{4}$$

$$\varphi = 26.5 - 37.4(1 - NPHI - V_{Shale}) + 62.1(1 - NPHI - V_{Shale})^2 \tag{5}$$

$$V_{Shale} = \frac{GR - GR_{\min}}{GR_{\max} - GR_{\min}} \tag{6}$$

$$C_o = \frac{UCS(1 - \sin\varphi)}{2\cos\varphi} \tag{7}$$

The tensile strength ($T_o$) corresponds to the ability of the rock to support tensile failure. The rock materials fail in a sudden and brittle manner at stress magnitudes of only 1/12 to 1/8 of their unconfined compressive strength (*UCS*) (Chang et al., 2013).

**Formation Pore Pressure**

Two methods (i.e., direct and indirect) are often employed in the petroleum industry to determine pore pressure. Direct measurement methods use well test techniques, such as the drill stem test (DST) and repeated formation test (RFT), to measure formation pore pressure for specific depths, whereas indirect (i.e., empirical and theoretical) methods are based on petrophysical data that are developed to predict pore pressure along the well length (Zhang, 2011). For more confidence, the estimated formation pore pressure from indirect methods is usually validated with the available measured formation pressure points of the DST or RFT. Eaton's (1969) equation is conventionally applied to predict the formation pore pressure based on the sonic wireline measurements. This equation is formulated as:

$$P_{pg} = OBG - (OBG - P_{hg})\left(\frac{NCT}{DTCO}\right)^3 \tag{8}$$

**Vertical Stress**

In areas with low tectonic activity, vertical stress represents the weight of overlying formations (Jaeger et al., 2007). The vertical stress was calculated by integrating the bulk density log over the vertical depth, using Eq. 9.

$$\sigma_v = \int_0^z \rho(z) g dz \tag{9}$$

Where, $g$ represents the acceleration constant due to gravity (m/s$^2$), $z$ is the vertical depth (m), and $\rho$ is the rock bulk density (g/cm$^3$).

**Horizontal Stresses (Minimum and Maximum)**

The poro-elastic horizontal strain is perhaps the most commonly used method for horizontal principal stress estimation (Gholami et al., 2017). For a fluid-saturated porous material that is assumed to be linear, elastic, and isotropic, considering anisotropic tectonic strain, the horizontal stresses (minimum and maximum) are expressed in Eqs. 10 and 11, respectively (Thiercelin and Plumb, 1994).

$$\sigma_h = \frac{v}{1-v}\sigma_v + \frac{1-2v}{1-v}\alpha P_p + \frac{E}{1-v^2}\varepsilon_x + \frac{vE}{1-v^2}\varepsilon_y \tag{10}$$

$$\sigma_H = \frac{v}{1-v}\sigma_v + \frac{1-2v}{1-v}\alpha P_p + \frac{E}{1-v^2}\varepsilon_y + \frac{vE}{1-v^2}\varepsilon_x \tag{11}$$

In the above equations, $\alpha$ is Biot's coefficient, which is maintained at unity to account for the brittle failure of rocks (conventionally $\alpha = 1$), $\varepsilon_x$ is the strain in the minimum horizontal stress direction, and $\varepsilon_y$ is the strain in the maximum horizontal stress direction. The two horizontal strains ($\varepsilon_y$ and $\varepsilon_x$) can be measured by Eqs. 12 and 13, respectively (Kidambi and Kumar, 2016).

$$\varepsilon_y = \frac{\sigma_v v}{E}\left(1 - \frac{v^2}{1-v}\right) \tag{12}$$

$$\varepsilon_x = \frac{\sigma_v v}{E}\left(\frac{1}{1-v} - 1\right) \tag{13}$$

**Formation Fracture Pressure**

The fracture pressure (FP) is the amount of pressure necessary to open existent fractures or break the rock structure of a formation. In other word, it is the pressure level, above which drilling fluids are capable of inducing rock formation fractures hydraulically. The formation fracture pressure (FP) were calculated by Matthews–Kelly's equation (Das and Chatterjee, 2017).

$$FP = K_i(\sigma_v - PP) + PP \tag{14}$$

$$K_i = \frac{\sigma_h}{\sigma_v} \tag{15}$$

## Input Data Selection

The performance of ANNs is negatively highly affected by increasing the number of input parameters, so it is crucial to limit the number of inputs to maximize the efficiency of the model. In this study, the *f*scaret package of *R* environment was applied to justify the worth of the input parameters in predicting the amount of lost circulation (Szlek and Mendyk, 2018). This method is a simple package providing fast and automated feature ranking based on the caret package (Kazemi et al., 2016). Out of the 30 variables studied, 10 constant or nearly constant variables had to be excluded, and the remaining 20 variables were considered to be the input parameters to predict the amount of lost circulation, as shown in Table 1. The final selected input parameters consisted of 20 variables that are most consistent with the specifications given in the literature (Fig. 1).

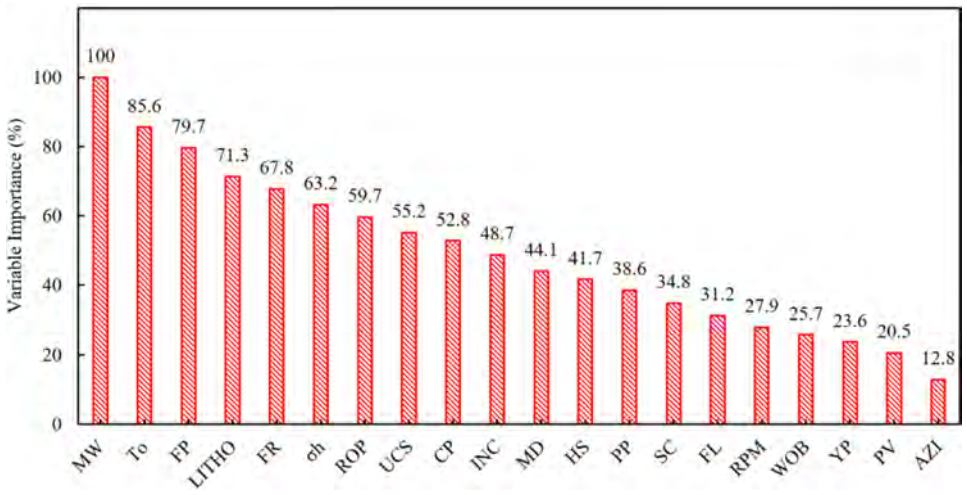


**Figure 1—Ranking of variables.**

**Table 1—Ranges of input parameters**

| Parameter | Minimum | Maximum |
|---|---|---|
| Mud weight (g/cc) | 1.02 | 1.35 |
| Tensile Strength (MPa) | 2.43 | 11.82 |
| Formation fracture pressure (MPa) | 28.3 | 44.8 |
| Lithology* | — | — |
| Flow rate (l/min) | 500 | 2500 |
| Minimum horizontal stress (MPa) | 22.1 | 35.7 |
| Rate of Penetration (m/hr) | 1 | 25 |
| Unconfined compressive strength (MPa) | 1.8 | 78.86 |
| Circulating pressure (psi) | 400 | 2381 |
| Inclination (degree) | 0 | 74 |
| Measured depth (m) | 406 | 3207 |
| Hole size (in) | 26 | 8.5 |
| Formation pore pressure (MPa) | 2.5 | 22.6 |
| Solids content (vol. %) | 1 | 28 |

| Parameter | Minimum | Maximum |
|---|---|---|
| Fluid loss ($cm^3$/min) | 1 | 25 |
| Rotation per minute (rev/min) | 40 | 200 |
| WOB (ton) | 1 | 27 |
| Yield point (g/100 $cm^2$) | 4 | 43 |
| Plastic viscosity (cp) | 5 | 39 |
| Azimuth (degree) | 0 | 360 |

*Lithology: Dolomite, Dolomite Limestone, Anhydrite, Gypsum, Limestone, Chalky Limestone, Marly Limestone, Argillaceous Limestone, Shaly Limestone, Sand & Gravel.

## Data Preprocessing

There are several ways to translate textual or symbolic data into numeric data. Unary encoding, numbering classes, and binary encoding are some of the common symbol translation techniques. Numbering classes were used in this study to translate the lithology type into a numeric form, as shown in Table 2.

**Table 2—Generated code for lithology type.**

| Lithology | Code |
|---|---|
| Dolomite | 0 |
| Dolomite Limestone | 1 |
| Anhydrite | 2 |
| Gypsum | 3 |
| Limestone | 4 |
| Chalky Limestone | 5 |
| Marly Limestone | 6 |
| Argillaceous Limestone | 7 |
| Shaly Limestone | 8 |
| Sand & Gravel | 9 |

Furthermore, the input data were normalized depending on either the transfer function applied in constructing the ANNs. Regarding the Feed-Forward Back-Propagation algorithm (FFBP) with LOGSIG transfer function, the normalization can be applied to fall input and target data in the range of 0 to +1. On the other hand, when TANSIG transfer function is used, the input and target data are scaled in the range of –1, to +1 (Jahanbakhshi et al., 2012).

## Model Performance Assessment

The common method for the model's validation is to split the dataset into training and test sets, and evaluate the performance based on the test set (Anemangely et al., 2019). Among 1,120 datasets of acquired data, which contained 20 input parameters and one output parameter (the amount of lost circulation), the ratio of 4:1was applied for training and testing the developed model, respectively. To assess the model prediction performance, the commonly used conventional performance indicators such as the root mean square error (RMSE), Average absolute percentage error (AAPE), and the correlation coefficients ($R^2$) between the measured value and the predicted value were adopted to evaluate the predictive accuracy of various models. The model which has a lower RMSE, AAPE and higher $R^2$, can be considered as the best model.

$$RMSE = \sqrt{\frac{1}{n}\sum_{i=1}^{n}(f(x_i) - y_i)^2} \tag{16}$$

$$AAPE = [\frac{1}{n}\sum_{i=1}^{n}\frac{|x_i - y_i|}{x_i}]*100 \tag{17}$$

$$R^2 = 1 - \frac{\sum_{i=1}^{n}(f(x_i) - y_i)^2}{\sum_{i=1}^{n} f(x_i)^2 - \sum_{i=1}^{n}(y_i)^2/n} \tag{18}$$

## Artificial Neural Networks (ANNs)

Neural networks are information processing systems that are a rough approximation and simplified simulation of a biological learning process and have performance characteristics similar to those of biological neural networks. It is composed of a large number of highly interconnected processing elements (neurons) working in unison to solve specific problems. ANNs are configured for a specific application, such as pattern recognition or data classification, through a learning process (Miri et al., 2007).

The network structures of ANNs are made up of a number of neurons which are distributed in layers based on their different functions. Generally, a complete neural network consists of three different types on layers, namely, an input layer, one or more hidden layers, and an output layer in which each layer includes a preset number of neurons (Shi et al., 2016). The challenging step in ANNs modeling is tuning of theses parameters, which is mostly done by try and error technique. In ANNs, arriving signals (inputs) to each neuron in hidden layers, are multiplied by the adjusted weight elements ($w_{1j}$ … $w_{nj}$), combined, and then flow forward through a transfer function to produce the outputs for neurons (Eskandarian et al., 2017). Fig. 2 illustrates a scheme of a single neuron in ANNs modeling.

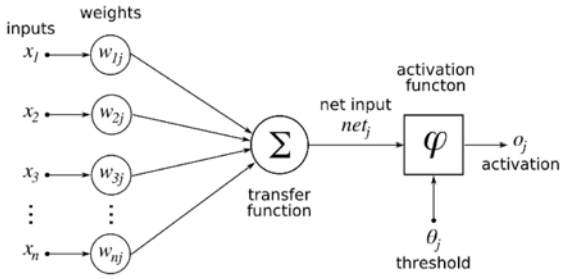


**Figure 2—Typical scheme of a single artificial neuron.**

For supervised learning, a back-propagation algorithm with a Levenberg-Marquardt training function is probably the best-known learning algorithm for neural networks (Aalizad and Rashidinejad, 2012). In this scheme, the network learns a predefined set of input-output sample pairs by using a two-phase propagate-adapt cycle (Abbas et al., 2018b). After the input data are provided as a stimulus to the first layer of the network unit, it is propagated through each upper layer until the output is generated. The latter is then compared to the desired output, and an error signal is computed for each output unit (Amer et al., 2017). The error signals are transmitted backward from the output layer to each node in the hidden layer that mainly contributes directly to the output. Each unit in the hidden layer receives only a portion of the total error signal, based roughly on the relative contribution the unit made to the original output.

To investigate the structure of the FFBP, various numbers of hidden layers and hidden neurons as well as different transfer functions were compared based on RMSE. The TANSIG and LOGSIG transfer functions

were examined for one, two, and three hidden layers. For the TANSIG transfer function, the RMSE reached its lowest value at 1.53 with 40 nodes and two hidden layers, while the RMSE attained its lowest point at 2.78 with 42 nodes and three hidden layers for the LOGSIG transfer function. Comparing the RMSE performance for all the developed structures of the FFBP indicated that the architecture of 40 neurons in two hidden layers with the TANSIG transfer function yielded the best efficiency in predicting the amount of lost circulation. Figures 3a and 3b present cross-plots of the predicted versus the actual amount of lost circulation for the developed model for the training and testing datasets, respectively. The ANNs model achieved a high $R^2$ of 0.92 for the training dataset, while $R^2$ was found to be 0.94 for the testing dataset. In addition, error distribution plots were also used to allow more statistical analysis of ANNs performance (Figs. 4a and 4b). Mean and standard deviation (SD) were equal of −0.02 and 1.24 for training dataset, while the mean and standard deviation (SD) were equal of 0.06 and 1.25 for the testing dataset. Small values of mean and standard deviation (SD) verify the robustness of the ANNs model. The error distribution indicates 81% of the predicted amount of lost circulation values have errors in the range of ±1 $m^3$/hr at the training phase, while 84% of predicted losses rate values have errors in the range of ±1 $m^3$/hr at the testing phase which is an acceptable error for the amount of lost circulation. To demonstrate the robustness of the proposed ANNs model, the RMSE, AAPE, and $R^2$ were calculated for the training and testing datasets (Table 3).

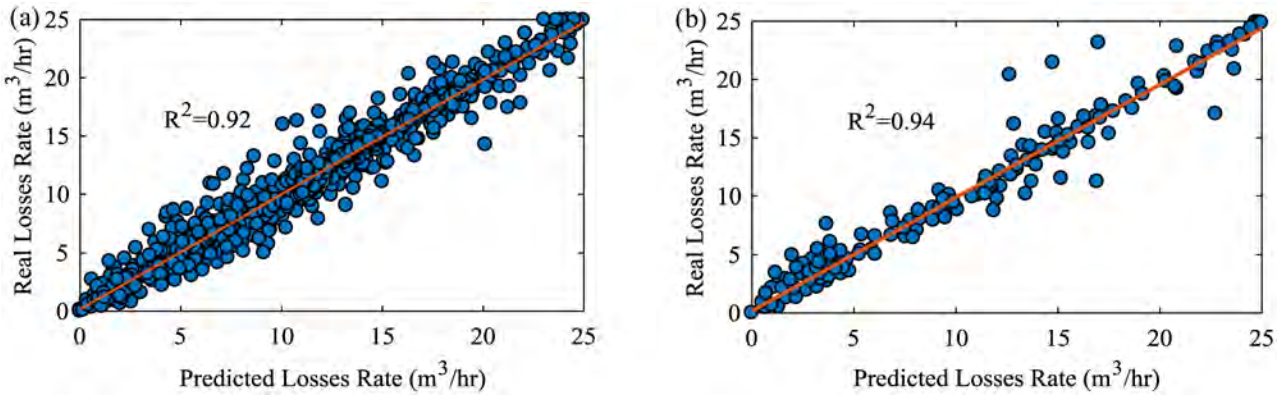


**Figure 3—Model outputs vs. real data: (a) training dataset, (b) testing dataset.**

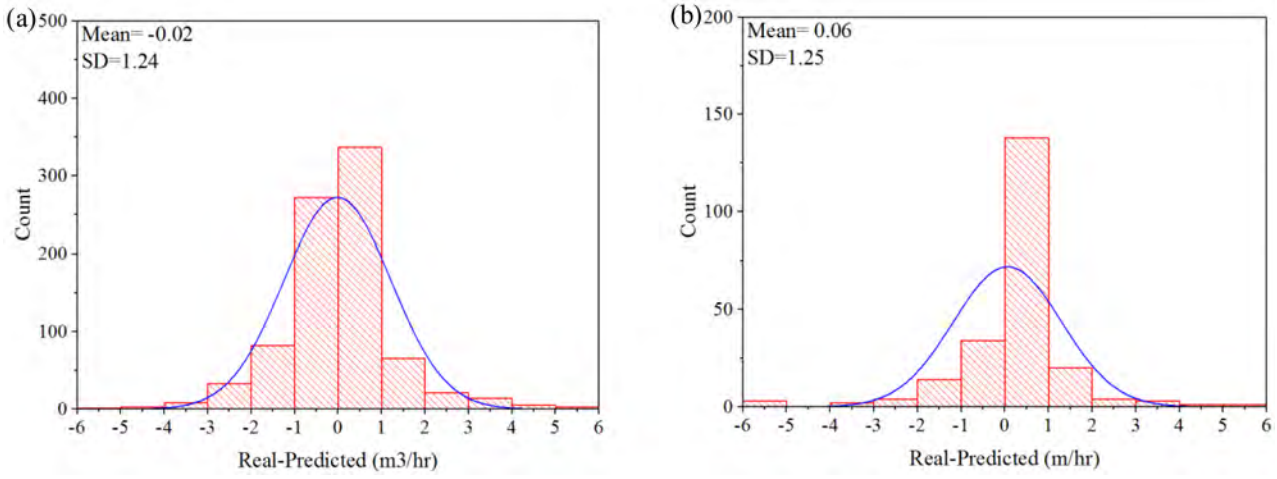


**Figure 4—Error distribution statistics for the developed ANNs model: (a) training dataset, (b) testing dataset.**

**Table 3—Prediction performance of the proposed ANNs models**

| Dataset | Performance Indicator | ANNs |
|---|---|---|
| Training | RMSE | 1.53 |
| | AAPE | 10.1% |
| | $R^2$ | 0.92 |
| Testing | RMSE | 1.38 |
| | AAPE | 9.6% |
| | $R^2$ | 0.94 |

## Effect of Operating Parameters on the Loss Severity

The impact of the most effective controllable drilling parameters (i.e., ROP, FR, CP, WOB, and RPM) was investigated to determine their effect on the loss severity according to the dataset used in this study. Figure 4 shows the impact of these variables on the amount of lost circulation; for each of these variables, the other variables were kept constant at their midrange or recommended values (Table 4), while the parameters under study (i.e., ROP, FR, CP, WOB, and RPM) varied within the range of the input parameters used in the ANNs training process.

**Table 4—Constant values of input parameters**

| Parameter | Fixed Value |
|---|---|
| Mud weight (g/cc) | 1.16 |
| Tensile Strength (MPa) | 6 |
| Formation fracture pressure (MPa) | 38.5 |
| Lithology | Limestone |
| Flow rate (l/min)* | 1500 |
| Minimum horizontal stress (MPa) | 30 |
| Rate of Penetration (m/hr)* | 5 |
| Unconfined compressive strength (MPa) | 60 |
| Circulating pressure (psi)* | 1000 |
| Inclination (degree) | 30 |
| Measured depth (m) | 2900 |
| Hole size (in) | 12.25 |
| Formation pore pressure (MPa) | 13.5 |
| Solids content (vol. %) | 8 |
| Fluid loss ($cm^3$/min) | 15 |
| Rotation per minute (rev/min)* | 100 |
| WOB (ton)* | 9 |
| Yield point (g/100 $cm^2$) | 18 |
| Plastic viscosity (cp) | 14 |
| Azimuth (degree) | 240 |

*Parameter under study is varied.

Figures 5a and 5b demonstrate a semi-straight line response of the losses rate to the ROP and FR, respectively. Applying very fast ROP results in improper hole cleaning and negatively effect on the loss severity. In addition, an excess amount of FR causes a positive effect on the hydraulic impact force

by increasing the equivalent circulating density (ECD), which increases the losses rate. The relationship between the losses rate and CP is presented in Fig. 5c. An increase in the CP generally tends to increase in the losses rate slightly, but a significant increase in the losses rate was seen at a high CP of more than 1500 psi. This behavior may happen because of the influence of CP on the hydraulic impact force. Figures 5d and 5e show that the losses rate is directly proportional to the WOB and RPM, where increasing the WOB and RPM will push the bit cutters further down into a formation and raise the shearing force of the cutters to disintegrate more rocks and therefore increase the ROP, which subsequently leads to increase the losses rate. This deterioration continued until the point at which rapid bit-wearing occurred and reversed the result.

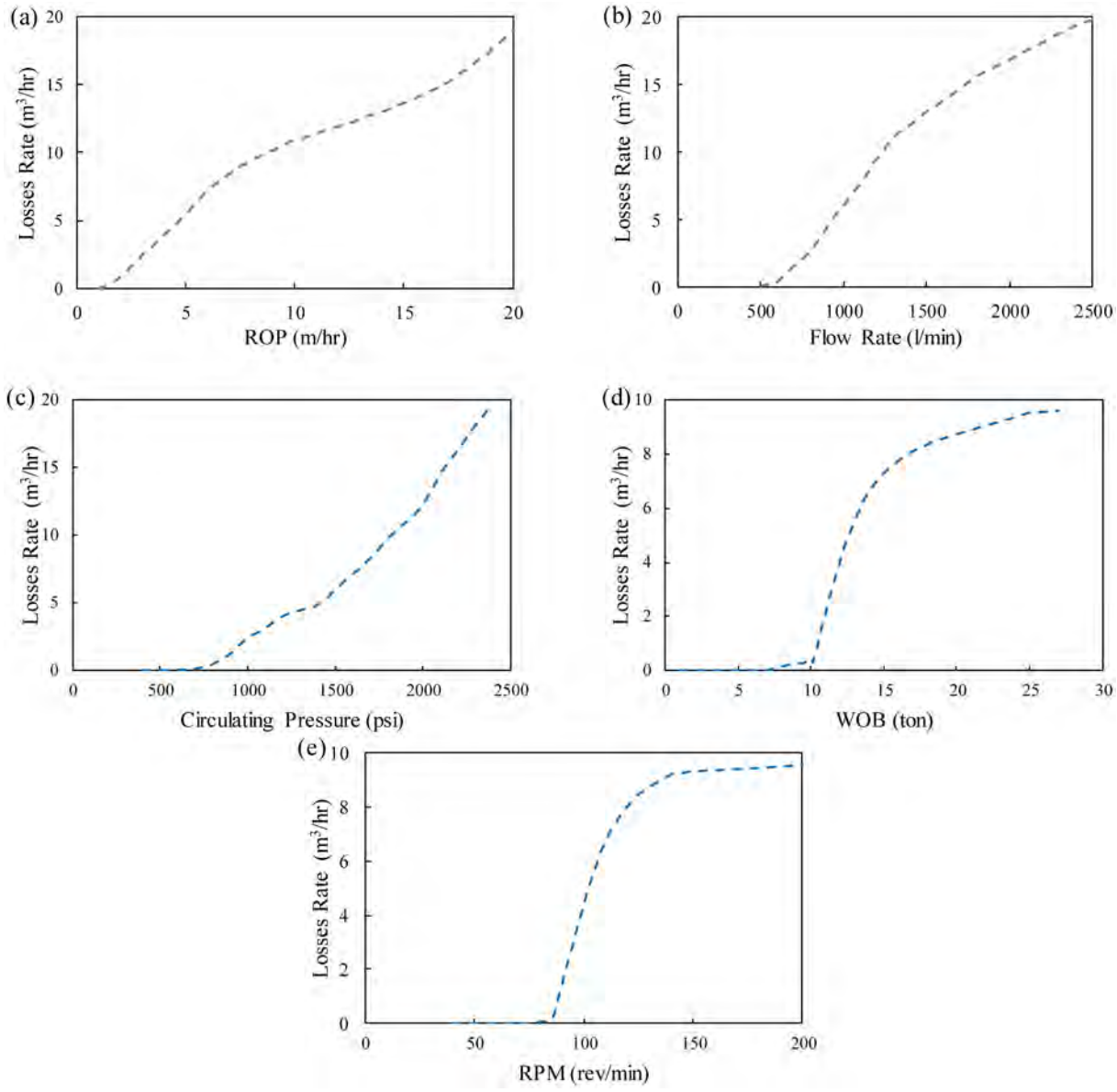


**Figure 5—Effect of operating parameters on the loss severity: (a) effect of the ROP, (b) effect of the FR, (c) effect of the CP, (d) effect of the WOB, and (e) effect of the RPM.**

## Simulating the Losses Rate

A simulation was conducted using the collected datasets to predict the losses rate for two wells (i.e., wells numbered 1 and 2) (Figs. 6 and 7, respectively). The validity of these parameters was first examined to remove outlier data. For this purpose, the measured data values of drilling parameters were statistically

compared to normal operating values and plotted to facilitate the process of discovering unusual values and define outliers. The drilling parameter values were examined to remove all records that have unusual values. The predicted losses rate was compared to the actual losses rate and introduced as a function of the measured depth (MD). To visualize the quality of the prediction, predicted penetration rates and residual errors by different models are compared with the measured ones for the overall data set. The results show a reasonable match between the predicted and actual losses rate, which indicates the success of modeling with a machine learning approach and of the entire procedure undertaken by this study.

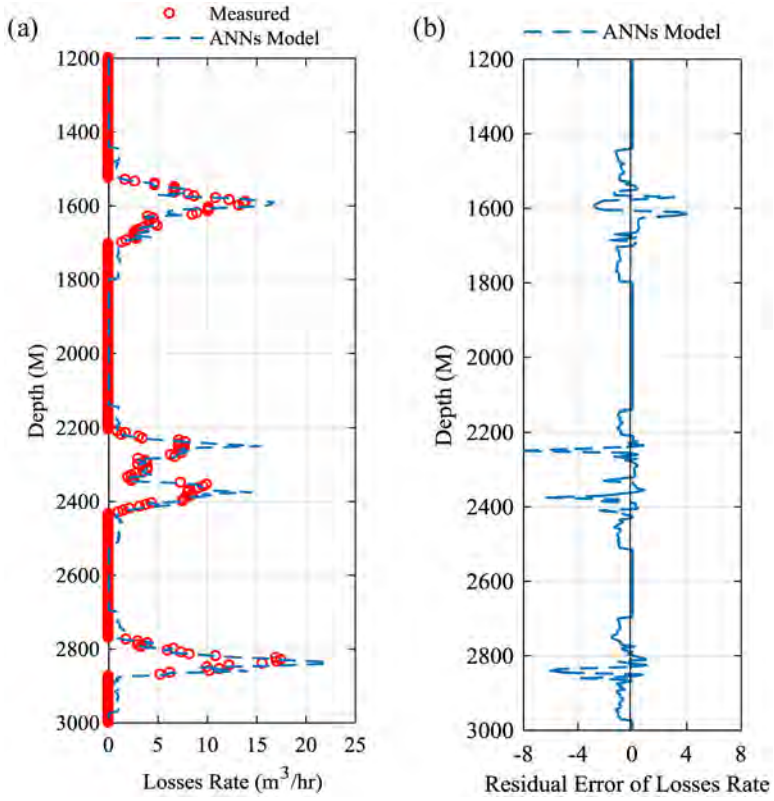


**Figure 6—Losses rate prediction for well 1: (a) predicted and measured losses rate along the depth, (b) residual errors of the predicted losses rate.**

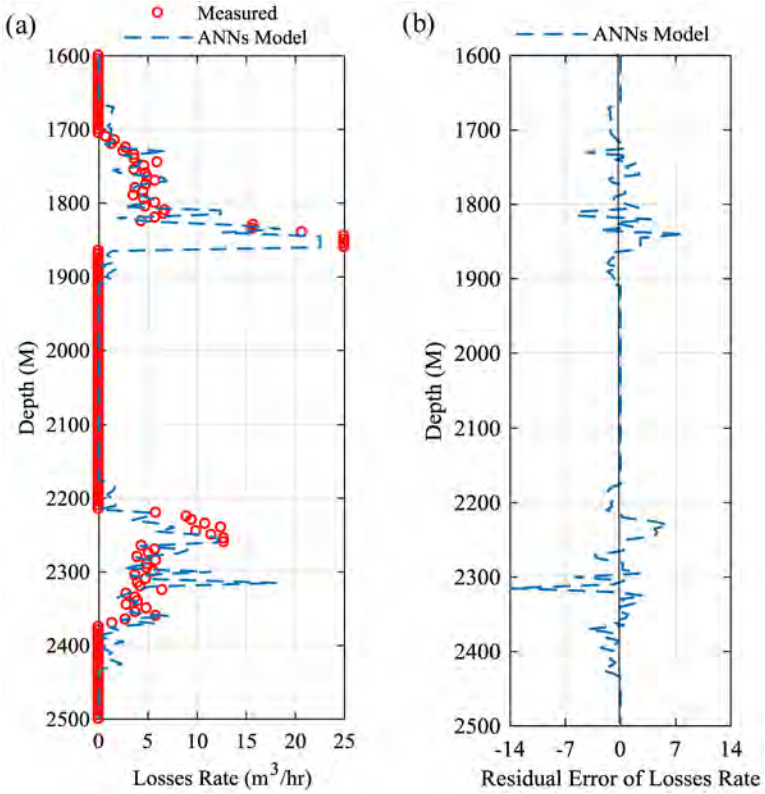


**Figure 7—Losses rate prediction for well 2: (a) predicted and measured losses rate along the depth, (b) residual errors of the predicted losses rate.**

## Conclusions

A methodology was proposed for prediction of lost circulation in any coordinates of field using operational variables and geological parameters. According to the results of feature ranking, mud weight, tensile Strength, and formation fracture pressure had the most impact on the amount of lost circulation. ANNs showed reasonable values of RMSE, AAPE, and $R^2$ during the training and testing process. The ANNs model with 20 variables was the most accurate model among all (RMSE of 1.53 and 1.38 for training and test model, respectively). Furthermore, the effect of the controlled drilling parameters (i.e., ROP, CP, FR, WOB, and RPM) on the losses rate was investigated to determine how they performed within the dataset. The consequences were similar to those achieved from field experiments. Therefore, it can be concluded that the model provides an efficient tool for determining the effect of these variables on the losses rate within realistic technological constraints.

## Acknowledgments

The authors would like to gratefully acknowledge Basrah Oil Company (BOC), Missan Oil Company (MOC), and Iraqi Drilling Company (IDC) in Iraq for providing technical data and their permission to publish the results.

## References

Aalizad, S. A., and Rashidinejad, F., 2012. Prediction of penetration rate of rotary-percussive drilling using artificial neural networks – a case study. *Arch. Min. Sci.*, **57** (3), 715–728. https://doi.org/10.2478/v10267-012-0046-x.

Abbas, A. K., Alameedy, U., Alsaba, M., and Rushdi, S. 2018a. Wellbore Trajectory Optimization Using Rate of Penetration and Wellbore Stability Analysis. Presented at the SPE International Heavy Oil Conference and Exhibition, Kuwait City, Kuwait, 10-12 December. http://dx.doi.org/10.2118/193755-ms.

Abbas, A. K., Flori, R. E., and Alsaba, M. 2019b. Stability Analysis of Highly Deviated Boreholes to Minimize Drilling Risks and Nonproductive Time. *Journal of Energy Resources Technology*, **141**(8), 082905. http://dx.doi.org/10.1115/1.4042733.

Abbas, A. K., Rushdi, S. and Alsaba, M. 2018b. Modeling Rate of Penetration for Deviated Wells Using Artificial Neural Network. Presented at the Abu Dhabi International Petroleum Exhibition and Conference (ADIPEC), Abu Dhabi, UAE, 12–15 November. https://doi.org/10.2118/192875-ms.

Abbas, A. K., Al-haideri, N. A., Bashikh, A. A., 2019a. Implementing Artificial Neural Networks and Support Vector Machines to Predict Lost Circulation. *Egyptian Journal of Petroleum*.

Agin, F., Khosravanian, R., Karimifard, M., and Jahanshahi, A., 2019. Application of adaptive neuro-fuzzy inference system and data mining approach to predict lost circulation using DOE technique (Case study: Maroon oilfield). *Petroleum*. http://dx.doi.org/10.1016/j.petlm.2018.07.005.

Alkamil, E. H., Abbas, A. K., Flori, R., Silva, L. E., Wunsch, D. C., and Chumkratoke, C., 2018. Learning from experience: Real-time H2S monitoring system using fuzzy ART unsupervised learning. Presented at the IADC/SPE Asia Pacific Drilling Technology Conference and Exhibition, Bangkok, Thailand, 27–29. http://dx.doi.org/10.2118/191097-ms.

Alsaba, M., Al Dushaishi, M. F., Nygaard, R., Nes, O., and Saasen, A., 2017. Updated criterion to select particle size distribution of lost circulation materials for an effective fracture sealing. *J. Pet. Sci. Eng.*, **149**, 641–648. http://dx.doi.org/10.1016/j.petrol.2016.10.027.

Amer, M. M., Dahab, A. S., and El-Sayed, A. H., 2017. An ROP Predictive Model in Nile Delta Area Using Artificial Neural Networks. Presented at the SPE Kingdom of Saudi Arabia Annual Technical Symposium and Exhibition, Dammam, Saudi Arabia, 24-27 April. http://dx.doi.org/10.2118/187969-ms.

Anemangely, M., Ramezanzadeh, A., Amiri, H., and Hoseinpour, S., 2019. Machine learning technique for the prediction of shear wave velocity using petrophysical logs. *J. Pet. Sci. Eng.*, **174**, 306–327. http://dx.doi.org./10.1016/j.petrol.2018.11.032.

Chang, C., Jo, Y., Oh, Y., Lee, T. J., and Kim, K., 2013. Hydraulic fracturing in situ stress estimations in a potential geothermal site, Seokmo Island, South Korea. *Rock Mech. Rock Eng.*, **47** (5): 1793–1808. http://dx.doi.org/10.1007/s00603-013-0491-7.

Chang, C., Zoback, M. D. and Khaksar, A., 2006. Empirical Relations between Rock Strength and Physical Properties in Sedimentary Rocks. *J. Pet. Sci. Eng.*, **51** (3–4): 223–237. http://dx.doi.org/10.1016/j.petrol.2006.01.003.

Chen, Y., Yu, M., Miska, S., Ozbayoglu, E., Zhou, S., and Al-Khanferi, N., 2017. Fluid flow and heat transfer modeling in the event of lost circulation and its application in locating loss zones. *J. Pet. Sci. Eng.*, **148**, 1–9. http://dx.doi.org/10.1016/j.petrol.2016.08.030.

Das, B., and Chatterjee, R., 2017. Wellbore stability analysis and prediction of minimum mud weight for few wells in Krishna-Godavari Basin, India. *Int. J. Rock Mech. Min. Sci.*, **93**, 30–37. http://dx.doi.org/10.1016/j.ijrmms.2016.12.018.

Davoodi, S., Ramazani S.A., A., Jamshidi, S., and Fellah Jahromi, A., 2018. A novel field applicable mud formula with enhanced fluid loss properties in High Pressure-High Temperature well condition containing pistachio shell powder. *J. Pet. Sci. Eng.*, **162**, 378–385. http://dx.doi.org/10.1016/j.petrol.2017.12.059.

Eaton, B. A., 1969. Fracture gradient prediction and its application in oilfield operations. *J. Petrol. Tech.*, **21** (10): 1353–1360. http://dx.doi.org/10.2118/2163-pa.

Eskandarian, S., Bahrami, P., and Kazemi, P., 2017. A comprehensive data mining approach to estimate the rate of penetration: Application of neural network, rule based models and feature ranking. *J. Pet. Sci. Eng.*, **156**; 605–615. https://doi.org/10.1016/j.petrol.2017.06.039.

Ezeakacha, C. P., and Salehi, S., 2018. Experimental and statistical investigation of drilling fluids loss in porous media–part 1. *J. Nal. Gas Sci. Eng.*, **51**, 104–115. http://dx.doi.org./10.1016/j.jngse.2017.12.024.

Feng, Y., and Gray, K., 2017. Review of fundamental studies on lost circulation and wellbore strengthening. *J. Pet. Sci. Eng.*, **152**, 511–522. http://dx.doi.org/10.1016/j.petrol.2017.01.052.

Gholami, R., Aadnoy, B., Foon, L. Y., Elochukwu, H., 2017. A methodology for wellbore stability analysis in anisotropic formations: A case study from the Canning Basin, Western Australia. *J. Nal. Gas Sci. Eng.*, **37**, 341–360. http://dx.doi.org/10.1016/j.jngse.2016.11.055.

Helaleh, A., and Alizadeh, M., 2016. Performance prediction model of miscible surfactant-CO2 displacement in porous media using support vector machine regression with parameters selected by ant colony optimization. *J. Nal. Gas Sci. Eng.*, **30**, 388–404. http://dx.doi.org./10.1016/j.jngse.2016.02.019.

Jaeger, J. C., Cook, N. G., and Zimmerman, R. W., 2007. Fundamentals of Rock Mechanics, fourth ed. Wiley-Blackwell.

Jahanbakhshi, R., Keshavarzi, R., Aliyari Shoorehdeli, M., and Emamzadeh, A., 2012. Intelligent prediction of differential pipe sticking by support vector machine compared with conventional artificial neural networks: an example of Iranian offshore oil fields. *SPE Drill & Compl.*, **27** (04), 586–595. http://dx.doi.org/10.2118/163062-pa.

Kazemi, P., Khalid, M. H., Szlek, J., Mirtič, A., Reynolds, G. K., Jachowicz, R., and Mendyk, A., 2016. Computational intelligence modeling of granule size distribution for oscillating milling. *Powder Technol.*, **301**; 1252–1258. https://doi.org/10.1016/j.powtec.2016.07.046.

Kidambi, T., and Kumar, G. S., 2016. Mechanical earth modeling for a vertical well drilled in a naturally fractured tight carbonate gas reservoir in the Persian Gulf. *J. Pet. Sci. Eng.*, **141**, 38–51. http://dx.doi.org/10.1016/j.petrol.2016.01.003.

Li, Z., Chen, M., Jin, Y., Lu, Y., Wang, H., Geng, Z., and Wei, S., 2018. Study on intelligent prediction for risk level of lost circulation while drilling based on machine learning. Presented at the 52nd US Rock Mechanics/Geomechanics Symposium (ARMA), Seattle, Washington, 17–20 June.

Mansourizadeh, M., Jamshidian, M., Bazargan, P., and Mohammadzadeh, O., 2016. Wellbore stability analysis and breakout pressure prediction in vertical and deviated boreholes using failure criteria – A case study. *J. Pet. Sci. Eng.*, **145**, 482–492. http://dx.doi.org/10.1016/j.petrol.2016.06.024.

Miri, R., Sampaio, J. H., Afshar, M., and Lourenco, A., 2007. Development of Artificial Neural Networks to Predict Differential Pipe Sticking in Iranian Offshore Oil Fields. Presented at the International Oil Conference and Exhibition in Mexico. https://doi.org/10.2118/108500-ms.

Mohammed H. Q., Abbas, A. K., and Dahm, H. H., 2018. Wellbore instability analysis for Nahr Umr Formation in southern Iraq. Presented at 52nd US Rock Mechanics/Geomechanics Symposium (ARMA), Seattle, Washington, 17–20 June 2018.

Nasiri, A., Ghaffarkhah, A., Keshavarz Moraveji, M., Gharbanian, A., and Valizadeh, M., 2017. Experimental and field test analysis of different loss control materials for combating lost circulation in bentonite mud. *J. Nat. Gas Sci. Eng.*, **44**, 1–8. http://dx.doi.org/10.1016/j.jngse.2017.04.004.

Razavi, O., Karimi Vajargah, A., Van Oort, E., Aldin, M., and Govindarajan, S., 2016. Optimum particle size distribution design for lost circulation control and wellbore strengthening. *J. Nal. Gas Sci. Eng.*, **35**, 836–850. http://dx.doi.org./10.1016/j.jngse.2016.08.038.

Shi, X., Liu, G., Gong, X., Zhang, J., Wang, J., and Zhang, H., 2016. An Efficient Approach for Real-Time Prediction of Rate of Penetration in Offshore Drilling. *Mathematical Problems in Engineering*, 1–13. http://dx.doi.org/10.1155/2016/3575380.

Szlek, J, and Mendyk, A., 2018. Fscaret: Automated feature selection from "caret." https://cran.rproject.org/web/packages/fscaret/index.html (accessed 3 November 2018).

Thiercelin, M., and Plumb, R., 1994. A core-based prediction of lithologic stress contrasts in East Texas formations. *SPE Form. Eval.*, **9** (04), 251–258. http://dx.doi.org/10.2118/21847-pa.

Toreifi, H., Rostami, H., and Manshad, A. K., 2014. New method for prediction and solving the problem of drilling fluid loss using modular neural network and particle swarm optimization algorithm. *J. Petrol. Explor. Prod. Technol.*, **4** (4), 371–379. http://dx.doi.org/10.1007/s13202-014-0102-5.

Whitfill, D. L., Jamison, D. E., Wang, M., and Angove-Rogers, A., 2007. Preventing lost circulation requires planning ahead. Presented at the International Oil Conference and Exhibition in Mexico, Veracruz, Mexico, 27–30 June. http://dx.doi.org/10.2118/108647-ms.

Zhang, J., 2011. Pore pressure prediction from well logs: Methods, modifications, and new approaches. *Earth Sci. Rev.*, **108** (1–2): 50–63. http://dx.doi.org/10.1016/j.earscirev.2011.06.001.